HIGH RESOLUTION DAMAGE DETECTION OF LOADED CARBON/EPOXY LAMINATES USING SYNCHROTRON RADIATION COMPUTED TOMOGRAPHY

A. Scott[1*], W. Hepples[2], N. Kalantzis[3], P. Wright[1], M. Mavrogordato[1], I. Sinclair[1], S.M. Spearing[1]
[1] School of Engineering Sciences, University of Southampton, Southampton, UK
[2] Luxfer Gas Cylinders, Colwick, Nottingham
[3]Luxfer Gas Cylinders, Gerzat, France
* Corresponding author(anna.scott@soton.ac.uk)

1 Introduction

The inherent heterogeneity and anisotropy of polymer matrix composites leads to complex macro and micro-mechanical fracture behaviour. For relatively simple uni-directional materials, various micromechanical approaches exist to predict tensile failure, for example the strength distribution and stress transfer models of Rosen [1], Batdorf [2] and Hedgepeth [3], however experimental validation of model predictions at micromechanical length-scales is largely unavailable, undermining model confidence and potential for truly predictive use.

Established micromechanical analysis methods (e.g. optical microscopy electron microscopy, acoustic emission) may be considered somewhat limited, having one or more of the following constraints; surface-only assessment, destructive, time consuming, poor spatial resolution and/or mechanistically ambiguous. High resolution computed tomography (CT) can overcome many of these problems, providing a resolution that allows damage mechanisms down to the single-fibre level to be quantified in three dimensions (3D).

In the present work, high-resolution synchrotron radiation CT results have been obtained for two carbon/epoxy composite laminate structures. The imaging techniques enable all major damage mechanisms to be identified and quantified, with the present work particularly focusing on individual fibres breaks. A detailed physical insight into the failure processes of cross-ply laminated flat plate and circular hoop structure is obtained, providing experimental data for direct theoretical model comparison.

2 Materials and Method

Two sample types were tested, consisting of a notched laminate tensile sample (T700G/epoxy) and an internally pressurised hoop structure (T700S/epoxy).

2.1 Notched Sample

The $[90/0]_s$ notched plates were fabricated from Hexcel Hex-Ply M21 T700G carbon fibre pre-preg, with a nominal fibre volume fraction of 60% to the manufacture's specifications. The double notched tensile samples were prepared via waterjet cutting, as reported by Wright et al. [4], see **Figure 1**.

The notched samples were loaded *in-situ* to failure. The average ultimate tensile failure stress, σ_{uts}, was found to be 910MPa across the notch section (based on four specimens). Tests were carried out at the ID19 beamline at the European Synchrotron Radiation Facilities (ESRF) in Grenoble. They were scanned prior to loading and then at incrementally increasing stress levels ranging from 30% σ_{uts} to the point of final failure.

The optics were set to provide an isotropic voxel resolution of $1.4\mu m$, with the sample-detector distance being set to $37mm$, falling within the near-field Fresnel diffraction regime (edge detection) with a beam energy of 20kV. 2D radiographs were recorded at 1500 angular positions over 180º of rotation (parallel beam conditions) via a 2048x2048 detector system. Further details of the imaging process are provided in [4], whilst **Figure 2** shows representative results obtained. Figure 2 a) shows a 3D image of the notched region, in which the composite material has been digitally removed to show segmented 0º splits and transverse ply cracks, b) and c) show the corresponding slices.

2.1 Hoop structures

The hoop structures consisted of an internal aluminium liner, with carbon T700S/epoxy (CFRP) and glass/epoxy (GFRP) outer layers. The CFRP layers have been investigated in this work as they contribute to the majority of the strength of the structure. They consist of combinations of hoop layers (~90º to the axis of the cylinder) and helical layers (~20º). The hoop structures were taken to incremental pressures (70, 80, 90, 95, 98 and 100%) of the mean burst pressure to capture the damage progression of the fibre breaks. The mean burst pressure was determined from 30 pre-burst test structures of the same layup and material.

Six AE sensors were applied to each hoop structure to capture AE signals and events during pressurisation. An AE event was located when at least four sensors detected an emission, on the basis of the time of arrival at each sensor and the speed of sound in the composite walls. The acoustic emission test procedure was informed by Kalantzis [5]. The signals were pre-amplified by 40dB and band-pass filtered outside the range of 100kHz to 1MHz to filter the background noise not associated with damage. The AE signals were recorded and analysed with a Vallen AMSY 4 data acquisition system.

A multi-scale imaging technique was then used to assess materials characteristics at the macro, meso and micro-scale. Micro-focus CT (µCT) has been used to provide images at moderate to low resolutions, shown in **Figure 3** (a) and (b), from whole component samples and sectioned sub-regions. The µCT images were taken using an X Tek Benchtop 160Xi scanner. In this system X-rays are generated by an accelerated electron beam falling on a metal target (typically tungsten). Due to the conical beam geometry, a smaller sized sample achieves higher resolution. At low geometrical magnifications the resolution is primarily limited by the number of pixels across the detector (~1200 in this case) and the width of the sample. The highest resolution (~3μm, limited by the spot size) is achievable for objects with a cross-section of ~3.6mm, with the largest objects imaged here (~90mm cross-section) yielding a voxel resolution of about 75μm.

In addition to µCT imaging of the hoop structures, high resolution imaging of critical regions of interest was carried out at the ESRF providing complementary information down to single fibre levels, as shown in **Figure 3**. Regions of interest were identified as areas of high energy and amplitude from the AE measurements, with samples being physically extracted via slow-speed diamond saw sectioning down to 2x2mm cross-section sticks

3 Analysis

3-D volumes were analysed using the commercial package VG studio Max v2.1 and features of interest were identified and segmented. Semi-automatic techniques were used to analyse cracks and fibre breaks. For cracks, an approximate region of interest was drawn around the feature to be segmented, a 3D seed growth tool was then used to capture more precisely the geometry and location. Fibre breaks were individually detected by the distinct bright fringes generated by phase contrast. To ensure fibre breaks are not mistaken for voids or imaging artefacts, orthogonal planes were carefully inspected, as shown in **Figure 4**.

For all load levels and both sample types, fibre failures were judged to be quite clear, with average crack openings well in excess of the voxel size. Average fibre break opening distances of 2.28μm were identified for the notched sample.

4 Results

4.1 Notched sample

Image analysis was carried out at multiple load steps leading to final failure. Previous work by Wright et. al. [4] and this study show matrix damage occurs in advance to fibre breaks. **Figure 5** shows the accumulation of fibre breaks with increasing load. When the acceleration in fibre break levels begins (beyond 70% of failure load), splitting and delamination have largely separated the central 0° ply in the near-notch region from the surrounding 90° plies.

The formation of clusters of fibre breaks with increasing load were observed and quantified, as

shown in Table 1. A cluster has been classified in this work as neighbouring breaks that occur within a transverse separation distance (*i.e.* perpendicular to main fibre direction) of less than the mean interfibre spacing in the transverse directions, and less than the ineffective length in the axial direction. The ineffective length was estimated as the smallest distance between fibre breaks that occur along the axis of the same fibre, as shown in **Figure 6**. The value of 70μm was considered to give a reasonable upper bound estimate of the ineffective length for the T700G notched samples.

No correlation was found between the location of matrix cracks in the 90° plies and fibre breaks in the 0° ply. At present qualitative visualisation has shown no overwhelming correlation between the location of fibre breaks and other micro-structural features, *e.g.* voids and resin rich regions, however the data obtained in this experiment gives scope for further statistical quantification that is currently ongoing.

3.2 Hoop Structure

To identify the progression of damage with increasing load, fibre breaks were manually counted within the carbon fibre hoop plies at each incremental pressure (qualitative inspection showed no fibre breaks in the helical layers). A significant number of fibre breaks were observed in the near burst samples (1548 breaks per mm^3 found in the highest fibre break density sample at 100% nominal burst).

To assess a variety of load conditions it was necessary to analyse smaller sub-volumes within the samples, corresponding to a region of ~0.5mm^2 by 1mm long within each carbon fibre hoop ply. Although this sub-volume is only a small part of the cylinder as a whole, it covers some 6500 individual fibres (and hence *~6.5m of total fibre length)*. To assess local variability, fibre breaks were also analysed for a larger volume within one loaded sample, with the variation of break density ranging from 1498 breaks per mm^3 for a volume of 1.13mm^3 and 1548 breaks per mm^3 for a volume of 0.5mm^3, *i.e.* ~3% variation.

Figure 7, shows the accumulation in fibre break density with increasing stress for both inner hoop wound layers and outer hoop layers of the samples tested. It can be seen that the density of fibre breaks is much higher in the inner hoop ply than the outer hoop ply, consistent with stress partitioning found in the FEA analysis of these structures [6]. The ratio of inner hoop break densities to outer hoop densities range in any one sample between 2.3 and 9.7, in which the inner hoop layer always contained more fibre breaks.

The incidence of fibre clusters was quantified, as reported for the notched sample. The minimum ineffective length estimate was found to be 26µm. Table 2 shows the clusters observed in samples taken to increasing levels of nominal burst, arranged in order of increasing number of fibre breaks. The variations in fibre break levels, particularly for the two samples at 100% nominal burst, maybe a associated with variations in burst pressures, attributable to some combination of local micro- and macro-structural variations.

3.3 Comparison between sample types

The accumulation of fibre breaks with increasing load for both sample types follow a similar power law curve. There appears to be more variance in the results for the pressure vessel sample, consistent with variations found in the microstructure.

The cluster formations with increasing load for both sample types evidenced much larger clusters in the notched laminate sample data. The largest cluster found was a 14plet, compared to a 4plet for the hoop structure samples. This is a much larger cluster particularly when 'normalised' in relation to the underlying incidence of singlet fibre breaks. For every singlet in the notched laminate sample there were evidently many more clusters compared with the pressure vessel samples.
Not only is the incidence of clustering different between samples, but the clustering 'shape' was also seen to differ: although the hoop structure samples were found to have a smaller estimated ineffective length than the notched sample (26μm compared to 70μm), the clusters in the hoop structure material frequently occurred with non-zero axial separations, as opposed to lying on the same plane, as was commonly the case with the notched laminate, suggesting that little or no effective fibre debonding

may be occurring in the tensile notched sample as clusters form.

Table 3 shows a comparison of the material properties of the two samples, indicating that the stiffness and tensile strengths are very similar. In this data, differences are found in the epoxy and the fibre sizing. The notched laminate has superior adhesion properties according to Toray Carbon Fibers America [7], whilst the epoxy also contains toughening particles. This improved adhesion may be expected to result in less debonding forming between the fibre and matrix interface [8]. Debonding can also be expected to reduce the stress concentration from the broken fibre onto the neighbouring fibres [9], which may then contribute to the reduced propensity for clustering in the hoop structure material. Although the notched samples contains toughening particles within the matrix, which may also be expected to reduce stress concentrations, **Figure 8** shows the toughening particles primarily lie within resin rich regions, whilst fibre clusters occur in the fibre rich regions (where the toughening particles are not present), and are therefore not expected to be significant in terms of cluster formation within the bulk of a given ply.

4 Conclusions

Imaging used in this study have enabled the first detailed volume-based quantification of the accumulation of broken fibres in two carbon/epoxy laminate systems up to a near failure condition. It has been found that failure of fibres is the dominant damage mechanism controlling tensile fracture stress. The incidence of fibre break clusters evidences the role of load sharing in the build up of a failure.

In both sample cases the accumulation of fibre breaks was found to follow a similar power law curve. Differences were found within the cluster formations, in which the notched sample composite material formed more numerous and larger break clusters that lay on the same planes. The hoop structure samples contained smaller clusters that were more separated along the axis of the fibres.

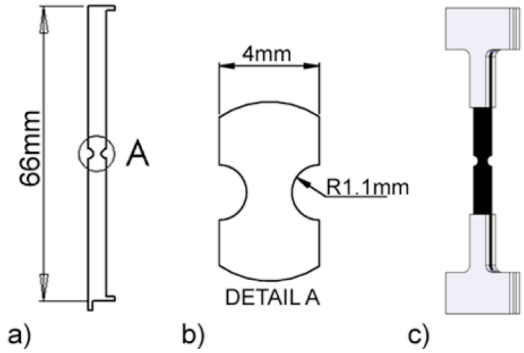

Figure 1: a) Notched sample geometry b) dimensions of the sample c) complete sample arrangement, with adhesively bonded aluminium end tabs [4]

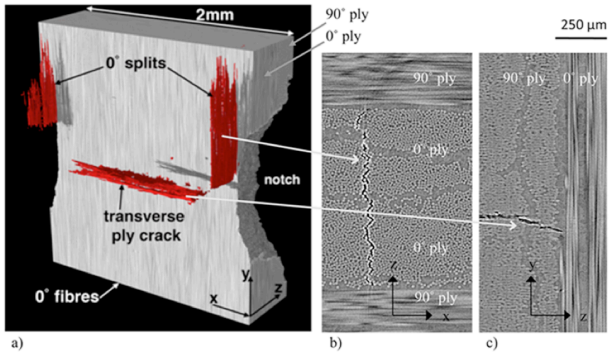

Figure 2: Representative SRCT imaging of matrix damage [4]: (a) 3D image of notched region, bulk of the composite digitally removed to reveal the damage (in red). (b) 2D slice showing a 0º ply split, and (c) transverse ply crack.

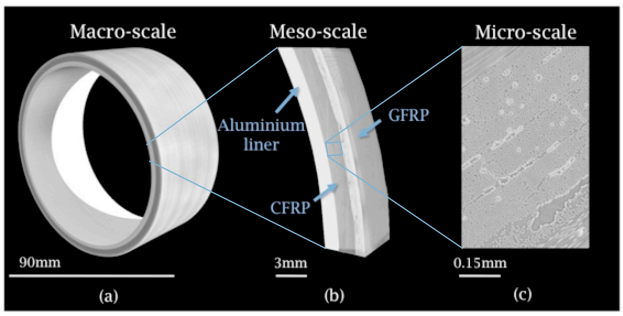

Figure 3: Multi-scale CT imaging approach of the composite/metallic structure: (a) and (b) µCT scans of whole structure and sub-region. (c) SRCT image of plies and local fibre distribution.

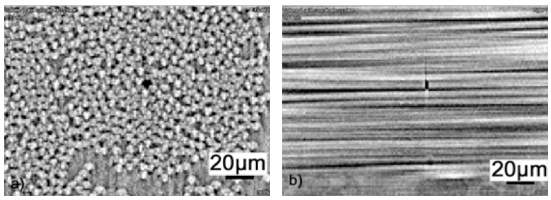

Figure 4: a) Axial and b) longitudinal views of the same fibre break.

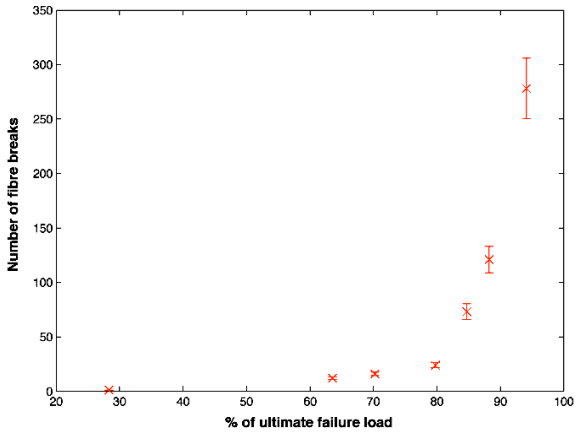

Figure 5: Accumulation of fibre breaks with increasing load for notched tensile sample. Error bars of average error in percent from three different recounts of the data.

% of Ultimate Failure	28	64	70	80	85	88	94
1plet	1	6	10	16	58	97	160
2plet		3	3	4	6	7	23
3plet					1	2	6
4plet						1	3
5plet							1
6plet							2
7plet							
8plet							
9plet							
10plet							
11plet							1
12plet							
13plet							
14plet							1

Table 1. Increasing cluster formation with load for notched tensile sample. An N plet consists of N, number of adjacent fibres breaks with a maximum axial separation of 70μm.

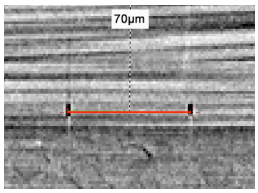

Figure 6: Example of two broken fibres occurring along the axis of the same fibre.

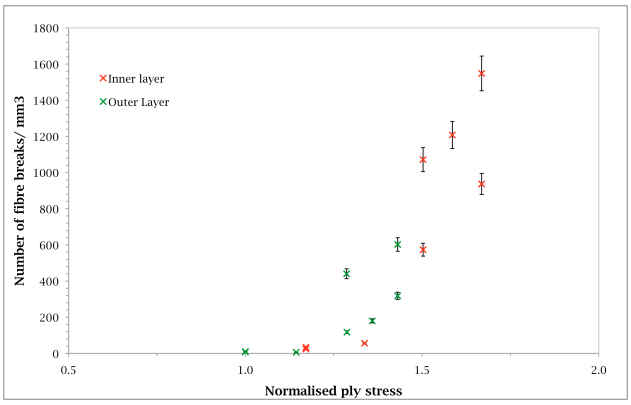

Figure 7: Accumulation of fibre breaks with increasing load for hoop structures. Error bars of average error in percent from three different recounts of the data.

% of Burst	70	80	90	100	98	95	100
1plet	15	29	267	422	445	530	728
2plet	1		8	23	17	28	18
3plet			2		1	4	2
4plet						3	1

Table 2: Increasing cluster formation with load for hoop structure, with a maximum axial separation of 26μm.

Sample	Fibre Type	Fibre tensile modulus GPa	Fibre tensile strength	Epoxy Type	Epoxy Modulus GPa
Pressure Vessel	T700S	230	4900	EPO 912	2.7
Notched Laminate	T700G	240	4900	HexPly M21	1.26

Table 3: Comparison of material properties for the hoop structure CFRP and the notched laminate

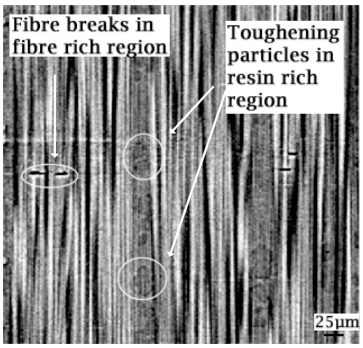

Figure 8: Notched laminate sample. Regions of toughening particles

References

[1] B. Rosen. "Tensile failure of fibrous composites". *AIAA journal,*Vol. 2, pp 1985–1991, 1964.

[2] S. B. Batdorf. "Tensile strength of unidirectionally reinforced composites". *International Journal of Reinforced Plastic Composites*, Vol. 1, pp 153–163, 1982.

[3] J.M. Hedgepeth. "Stress Concentrations in Filamentary Structures". *NASA TN D-882,* 1961.

[4] P. Wright, X. Fu, I. Sinclair, S. Spearing. "Ultra high resolution computed tomography of damage in notched carbon fibre-epoxy composites". *Journal of Composite Materials* Vol. 42, pp 1993–2002, 2008.

[5] N. Kalantzis. "Adaptive numerical modelling in the production of gas cylinders and associated technologies". *PhD. Thesis, University of Southampton*. 2008

[6] A. E. Scott, M. Clinch, W. Hepples, N. Kalantzis, I. Sinclair, S.M. Spearing "Advanced micro-mechanical analysis of highly loaded hybrid composite structures" *ICCM16, Edinburgh*, 2009.

[7] Toray Carbon Fibers America. Standard modulus carbon fibers, 2008. URL http://www.toraycfa.com/standardmodulus.html.

[8] G. A. Holmes, R. C. Peterson, D. L. Hunston, and W. G. McDonough. "E- glass/dgeba/m-pda single fiber composites: Interface debonding during fiber fracture". *Polymer Compos*., 28:561–574, 2007.

[9] X. F. Zhou and H. D. Wagner. "Stress concentrations caused by fiber failure in two-dimensional composites". *Compos. Sci. Technol*., 59(7):1063 –1071, 1999.